The Micelle-Bound Structure of an Antimicrobial Peptide Derived from the α-Chain of Bovine Hemoglobin Isolated from the Tick *Boophilus microplus*†

Maurício L. Sforça,‡ Alessandra Machado,§ Rita C. R. Figueredo,‡ Sérgio Oyama Jr.,‡ Fernanda D. Silva,|| Antonio Miranda,⊥ Sirlei Daffre,|| M. Terêsa M. Miranda,§ Alberto Spisni,*,‡,# and Thelma A. Pertinhez*,‡

Center for Molecular Structural Biology, Brazilian Laboratory of Synchrotron Light, Campinas, Brazil, Department of Biochemistry, Institute of Chemistry, and Department of Parasitology, Institute of Biomedical Sciences, University of São Paulo, São Paulo, Brazil, Department of Biophysics, Federal University of São Paulo, São Paulo, Brazil, and Department of Experimental Medicine, Section of Chemistry and Structural Biochemistry, University of Parma, Parma, Italy

Received November 23, 2004; Revised Manuscript Received March 4, 2005

ABSTRACT: Hemoglobin is known to be a source of peptides involved in several functions. The peptide FLSFPTTKTYFPHFDLSHGSAQVKGHGAK (Hb33−61) is a proteolytic product of the bovine hemoglobin α-chain found in the gut content of the cattle tick, *Boophilus microplus*, and it possesses antimicrobial activity. Since in the past we showed that the amidated form of Hb33−61, *Hb33−61a*, is active against a few Gram-positive bacteria and fungi strains at micromolar concentration [Fogaça et al. (1999) *J. Biol. Chem. 274,* 25330−25334], we have been prompted to shed more light on its functional and structural features. Here we show that the peptide is able to disrupt the bacterial membrane of *Micrococcus luteus* A270. As for its structure, it has a random conformation in water, and it does not interact with zwitterionic micelles. On the other hand, it binds to negatively charged micelles acquiring a finite structural organization. The 3D structure of *Hb33−61a* bound to SDS micelles exhibits a nonconventional conformation for an antimicrobial peptide. The backbone is characterized by the presence of a *β*-turn in the N-terminus and by a *β*-turn followed by a α-helical stretch in the C-terminus. A hinge, whose spatial organization is stabilized by side-chain−side-chain interactions, joins these two regions. Interestingly, it preserves structural features present in the corresponding segment of the bovine hemoglobin α-chain. *Hb33−61a* does not possess a well-defined amphipathic nature, and H/D exchange experiments show that while the C-terminal region is embedded in the SDS micelle, one face of the N-terminal half is partly exposed to the solvent.

Peptides with antimicrobial activity have been found in various organisms as plants, arthropods, fishes, amphibians, and mammals. Antimicrobial peptides (AMPs)[1] are part of the innate defense apparatus of living systems (*1*−*4*) against invading bacteria, fungi, and viruses. They may be produced constitutively or only after infection. Some are expressed under a tight gene regulation; others are the result of the processing of endogenous or exogenous mature proteins (*1*, *5*−*10*).

The structural motifs adopted by AMPs comprise the amphipathic α-helix, *β*-hairpins, *β*-sheet, or turns (*11*, *12*). As a result, an examination of the large collection of structural data available for antimicrobial peptides does not seem to evidence any formal relationship between structure or charge and activity (*13*). Accordingly, because of their diversity, it is difficult to categorize them. Nonetheless, based on their primary sequence and 3D structure, AMPs have been grouped into four main classes: (a) linear peptides with an amphipathic helix, (b) *β*-sheet stabilized by disulfide bridges, (c) peptides with the predominance of a certain amino acid in their sequence, and (d) peptides with loop structures (*10*).

Interestingly, despite such a structural heterogeneity, the AMP mechanism of action generally involves the invasion of the microorganisms through membrane disruption. However, it is also known that AMP may interfere with intracellular processes eventually via binding to targets in the bacteria cytoplasm (*14*−*16*).

Some of the AMPs described so far are products of the proteolysis of mature protein such as *β*-lactoglobulin (*17*,

† This research was partly supported by grants from the São Paulo State Research Foundation (FAPESP), Brazil, to A.S. (99/11030-9 and 99/07574-3), A.M. (00/03642-3), M.T.M.M. (01/11296-0), S.D. (98/11372-4), and T.A.P. (00/02026-7). A.M. (01/02270-8), M.L.S. (01/08095-3), and S.O.J. (01/08001-9) are recipients of postdoctoral fellowships from FAPESP.

* To whom correspondence should be addressed. T.A.P. and A.S.: Center for Molecular and Structural Biology, Brazilian Laboratory of Synchrotron Light; tel, ++55 19 3512 1119; fax, ++55 19 3512 1006; e-mail, thelma@lnls.br and alberto@lnls.br. A.S.: Department of Experimental Medicine, University of Parma; tel, ++39 0521 033807; fax, ++39 0521 033802; e-mail, aspin@unipr.it.

‡ Center for Molecular Structural Biology, Brazilian Laboratory of Synchrotron Light.

§ Department of Biochemistry, University of São Paulo.

|| Department of Parasitology, University of São Paulo.

⊥ Department of Biophysics, Federal University of São Paulo.

Department of Experimental Medicine, University of Parma.

[1] Abbreviations: AMP, antimicrobial peptide; CD, circular dichroism; DQF-COSY, double-quantum-filtered correlation spectroscopy; LPC, lysophosphatidylcholine; NMR, nuclear magnetic resonance; NOESY, nuclear Overhauser enhancement spectroscopy; PI, propidium iodide; RMSD, root mean square deviation; SDS, sodium dodecyl sulfate; TFE, 2,2,2-trifluoroethanol; TOCSY, total correlation spectroscopy.

10.1021/bi0475323 CCC: $30.25
Published on Web 04/06/2005

18), bovine α-casein (*19*), lactoferrin (*5*, *20*, *21*), ovalbumin (*22*), and hemoglobin (*6*−*8*, *23*, *24*).

It is long known that hemoglobin is a source of peptides that are involved in several biological functions (*25*). The existence of a hemoglobin fragment with antimicrobial activity was reported for the first time in 1999. It was isolated from the gut contents of the cattle tick, *Boophilus microplus* (*6*), and identified as a C-terminal carboxyl-free endogenous fragment of bovine hemoglobin encompassing the region 33−61 of the α-chain, Hb33−61. Its synthetic amidated form, *Hb33*−*61a*, exhibited a significant antibacterial and antifungal activity, while being practically inactive against eukaryotic cells such as bovine erythrocytes and the parasite *Leishmania amazonensis* (*26*, *27*). Subsequent reports documented the antimicrobial activity of intact hemoglobins of diverse origins (*23*) as well as of hemoglobins' derived AMPs obtained *in vitro* by cyanogen bromide digestion (*23*) or by pepsin hydrolysis (*24*). More recently, Nakajima et al. (*7*) found, in the midgut of another tick, *Ornithodoros moubata* (Acari: argasidae), two AMPs whose sequences correspond to residues 1−11 and 3−19 of rabbit hemoglobin α-chain, thus calling for a similar immune mechanism of defense in the two major families of ticks. Finally, Liepke and co-workers, searching in a human placental peptide library, isolated and identified two hemoglobin-derived AMPs (*8*), demonstrating the existence of natural hemoglobin fragments with antimicrobial activity also in humans. These peptides, that encompass residues 130−146 of human γ-hemoglobin and residues 111−146 of human β-hemoglobin, respectively, were also found in erythrocyte lysates. Moreover, being able to interact with lipopolysaccharides, they turned out to be active, at micromolar concentration, against both Gram-positive and Gram-negative bacteria as well as against yeast. Overall, these results suggested that the hemoglobin-derived AMPs may be important effectors of the innate immune response against microbial invaders.

Recognizing that C-terminal amidation either may increase the peptide resistance to protease (*28*) or may lead to the potentiation of its antimicrobial activity (*29*), and in view of the potential use of hemoglobin's derived AMPs as therapeutics in humans, we have been prompted to investigate in more depth the functional and structural features of the non-native amidated form of Hb33−61, *Hb33*−*61a* (*6*).

EXPERIMENTAL PROCEDURES

Peptide Synthesis. The peptide FLSFPTTKTYFPHFDL-SHGSAQVKGHGAK-NH_2 (*Hb33*−*61a*) has been synthesized, purified, and characterized as previously described (*6*).

Biological Activity. In situ viability assay was carried out using *Micrococcus luteus* A270 obtained from the Pasteur Institute Collection (Paris). The bacteria culture, in the middle of the logarithmic phase, was treated with the Live/Dead BacLight bacterial viability stain (L-7007; Molecular Probes, Eugene, OR) following the manufacturer's instructions. This kit utilizes a mixture of the green fluorescent nucleic acid stain, SYTO 9, with the red fluorescent nucleic acid stain, propidium iodide (PI). These stains differ not only in their spectral characteristics but also in their ability to penetrate healthy bacteria cells. In fact, SYTO 9 stains the DNA of all bacteria irrespective of whether they have the external membrane intact or damaged. In contrast, PI penetrates only bacteria with damaged external membranes, and it is also able to quench the fluorescence of SYTO 9. As a result, when bacteria are stained with a mixture of these two fluorescent dyes, the ones with intact cell membranes appear green, whereas the bacteria with damaged membranes turn out to be red. Briefly, the bacteria culture was incubated in Poor Broth nutrient medium (10^7 cells/mL) for 1 h at 30 °C in the presence or absence of 62.5 μM *Hb33*−*61a*. The peptide concentration used in the assay corresponds to 12.5 times its minimal inhibitory concentration (*6*). Subsequently, the culture was treated with a mixture of SYTO 9 and PI. The viability of the cells was analyzed using a Zeiss fluorescence microscope, Axiovert S100 (Germany), equipped with a digital camera, Hamamatsu C5810 (Sanyo Denki, Japan).

Circular Dichroism. Circular dichroism (CD) experiments were carried out using a Jasco 810 spectropolarimeter (Jasco International Co., Ltd.), coupled to a Peltier Jasco PFD-425S system for temperature control. Spectra collected in the far-UV region, 190−250 nm, were averaged over four scans, using a 1 mm path length quartz cell. Spectra collected in the near-UV region, 230−300 nm, were collected using a 1 mm path length quartz cell and averaged over eight scans. For the far-UV spectra, the peptide concentration used was 20 μM, and the measurements were performed either in aqueous solution or in the presence of variable concentrations of 2,2,2-trifluoroethanol (TFE), sodium dodecyl sulfate (SDS), or lysophosphatidylcholine (LPC) at various pHs. The pH was adjusted using small volumes of HCl or NaOH stock solutions. In the case of the near-UV spectra, the peptide concentration was 2 mM, and the measurements were carried out either in water solution or in the presence of 200 mM SDS, pH 4.0, at 20 and 37 °C. Following baseline correction, the measured ellipticity, θ (millidegrees), was converted to the molar mean residue ellipticity $[\theta]$ ($deg \cdot cm^2 \cdot dmol^{-1}$).

NMR Spectroscopy. The NMR samples were prepared by dissolving the lyophilized peptide *Hb33*−*61a* in 200 mM SDS-d_{25}/water solution to yield a final peptide concentration of 1.5 mM, pH 4.0. The ^1H NMR experiments were performed at 37 °C using a Varian INOVA 600AS spectrometer, operating at 599.68 MHz for the ^1H frequency. For sequential assignments and structure determination, TOCSY with 85 ms mixing time (*30*), NOESY with 200, 300, and 400 ms mixing times (*31*), and DQF-COSY (*32*) experiments were recorded. The water resonance was suppressed by using the WET sequence. Spectra were acquired with 1K complex data points in the acquisition domain and 512 increments in the time domain. The $^3J_{NH-\alpha}$ coupling constants were measured from the DQF-COSY spectra using a matrix of 8K × 2K. DSS (2,2-dimethyl-2-silapentane-5-sulfonate) was added to the sample as an internal standard and set at 0.00 ppm. The NMR data were processed with the Felix 2000 software (Accelrys Inc.) using a Silicon Graphics Octane 2 workstation. Resolution enhancement was achieved by apodization of the free induction decay with shifted square sine-bell window function. The data were zero-filled prior to Fourier transformation, and the baseline was corrected using a fifth-order polynomial function. Automated assignments of NOEs were obtained with the program st2 NMR (*33*). To obtain interproton distance constraints, the cross-peak volumes of the 300 ms NOESY spectra were measured and calibrated with respect to the cross-peak volume of geminal β-protons that correspond to an interproton distance

of 1.8 Å. The obtained NOE values were classified as strong, medium, and weak, corresponding to the upper bound distances of 2.8, 3.5, and 5.0 Å, respectively. The lower bound was taken to be the sum of the van der Waals radii (1.8 Å) for the interacting protons. The proton amide chemical shift temperature coefficients ($\Delta\delta_{NH}/\Delta T$) were obtained from a series of TOCSY spectra recorded every 5 °C in the temperature range 10−55 °C. The pK_a values of His45, His50, and His58 have been determined from a series of TOCSY ^{1}H NMR spectra carried out in the pH range 4.5−9.0. The pK_a values have been derived from a least-squares fit of the data to the Henderson−Hasselbach equation (see the Supporting Information).

H/D Exchange Experiments. A qualitative estimation of the labile amide hydrogen atoms of *Hb33−61a* in SDS micelles at 37 °C was obtained by hydrogen−deuteron (H/D) exchange experiments. The sample containing the peptide bound to the SDS micelles was lyophilized, and a D_2O/H_2O (9:1 v/v) solvent mixture was added immediately before acquiring a series of TOCSY spectra with duration of 5 h each (*34*).

Structure Calculations. The peptide three-dimensional structures, compatible with the experimental distance restraints, have been calculated using DYANA (*35*). The structures with a target function smaller than 0.22 ± 0.02 Å^2, with no distance violation larger than 0.2 Å and with no dihedral angle violation grater than 5°, were energy minimized with full consistent valence force field (*36*) (Morse and Lennard-Jones potentials, Coulombic term) by steepest descents and conjugated gradients using several thousand interactions until the maximum derivative was less than 0.001 kcal/Å. All calculations were carried out in a Silicon Graphics Octane 2 workstation using the DISCOVER (Accelrys, Inc.) software package, together with Insight II as a graphic interface. At the end, 20 models having the lowest energies out of the 40 starting structures were selected for structural analysis using PROCHECK-NMR (*37*).

RESULTS

Biological Activity. The effect of *Hb33−61a* on the viability of *M. luteus* was examined by fluorescence microscopy using a combination of the fluorochromes SYTO 9 and PI. As expected, the untreated cell culture showed only green fluorescence, indicating that exclusively SYTO 9 entered the bacteria (Figure 1a). In Figure 1b instead, one can appreciate that when the culture is treated with *Hb33−61a*, at a concentration of 62.5 μM, all bacteria exhibit a red fluorescence, indicating that the cell membrane has been damaged, allowing PI to enter the cell. As a control, we verified that bacterial membrane damaged by incubation with 100% 2-propanol showed only red fluorescence (data not shown).

Since these data show that *Hb33−61a* exerts its antimicrobial activity by permeabilizing the bacterial membrane, the description of its membrane-bound structure turns out to be a prerequisite to reach an understanding of its mechanism of action at a molecular level.

Circular Dichroism. The CD spectrum of *Hb33−61a* in aqueous solution at acidic pH shows a negative band at ∼198 nm that is typical of a peptide in random coil conformation

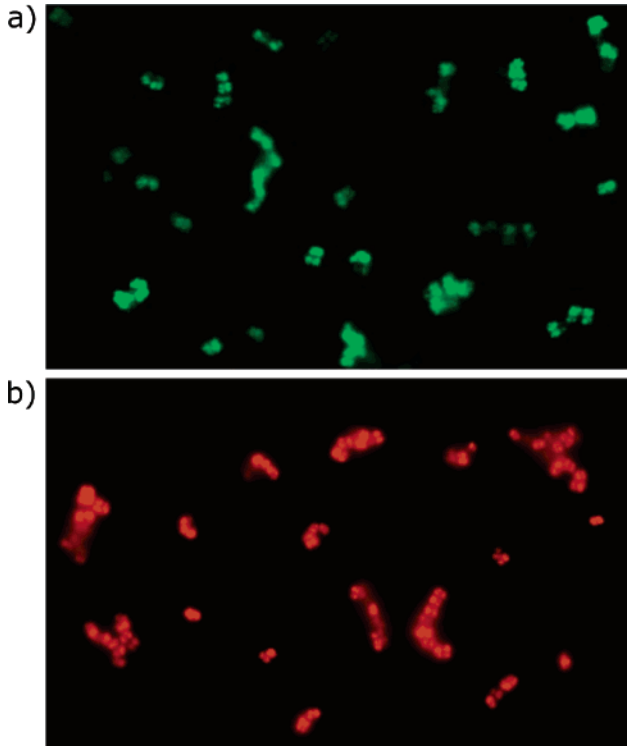

FIGURE 1: Viability of cells of *M. luteus* in the presence of *Hb33−61a* using the fluorescent dyes SYTO 9 and propidium iodide: (a) untreated culture; (b) culture treated with 62.5 μM *Hb33−61a*.

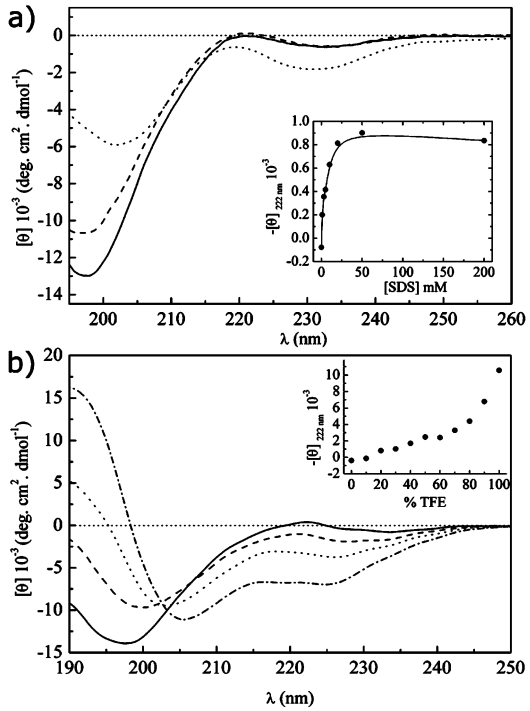

FIGURE 2: Far-UV CD spectra of (a) 20 μM *Hb33−61a* in aqueous solution (—), in the presence of 5 mM LPC (- - -), and in the presence of 200 mM SDS (···), pH 4.0, at 20 °C. Inset: Plot of $-[\theta]_{222}$ as a function of SDS concentration. (b) TFE titration of 20 μM *Hb33−61a*: (—) aqueous solution, (- - -) TFE/H_2O (30:70), (···) TFE/H_2O (70:30), and (—·—) TFE/H_2O (90:10). Inset: Plot of $-[\theta]_{222}$ as a function of TFE/H_2O (v/v) mixture.

(Figure 2a). The CD spectra carried out by varying the peptide concentration (20 μM−2 mM), the pH value (4−7 range), and the ionic strength (NaCl, 1−200 mM) evidenced

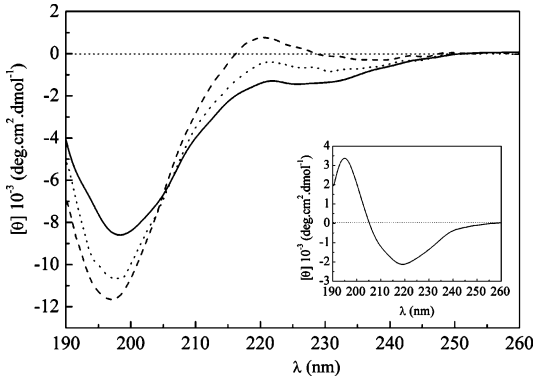

FIGURE 3: Far-UV CD spectra of 20 μM *Hb33−61a* in water, pH 4.0, at various temperatures: 10 °C (- - -), 35 °C (•••), and 70 °C (—). Inset: Difference spectrum between 70 and 10 °C.

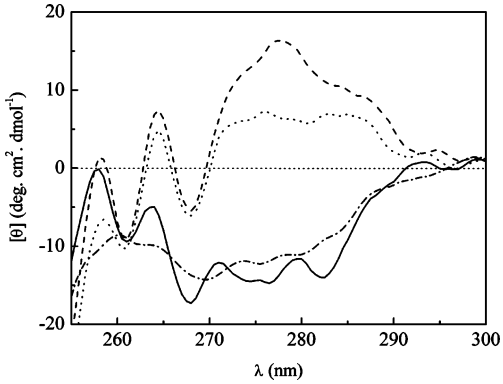

FIGURE 4: Near-UV CD spectra of 2.0 mM *Hb33−61a* in water, pH 4.0, at 20 °C (—) and 37 °C (—•—) and in the presence of 200 mM SDS, pH 4.0, at 20 °C (- - -) and 37 °C (•••).

that its secondary structure is insensitive to these experimental factors (data not shown).

On the other hand, the CD spectra obtained as a function of variable TFE/H_2O mixtures (v/v) revealed that the peptide is able to acquire an α-helical conformation (Figure 2b). Nonetheless, the fact that $[\theta]_{222}$ does not reach a plateau even at 100% TFE (inset of Figure 2b) suggests the absence of a two-state conformational transition. Having verified that the peptide conformation does not change in the pH interval 4−7, we inspected its structural features in the presence of membrane mimetics at acidic pH as these conditions were better suitable for the subsequent NMR experiments.

The addition of LPC micelles did not affect the CD spectrum of the peptide, indicating that it is not able to interact with zwitterionic micelles (Figure 2a). Differently, in the presence of SDS micelles (Figure 2a), we observed some changes in the CD spectrum such as a red shift of the band at 198 nm to about 202 nm and an increase of the negative broad band in the region 225−235 nm. The plot of $[\theta]_{222}$ against SDS concentration is reported in the inset of Figure 2a, and it shows that, already at 20 mM SDS, the peptide has reached a new stable conformation.

The spectral modifications induced by the addition of SDS (Figure 2a) point to the formation of turn elements (*38*) or to the onset of interactions between aromatic side chains (*39*, *40*), together with the induction of some helical secondary structure (about 24% as judged by the values of $[\theta]_{222}$; *41*).

Interestingly, the decrease in spectral intensity observed at high temperature in water (Figure 3) suggests that, as observed for other peptides (*42*), *Hb33−61a* undergoes an inverse temperature transition leading to the acquisition of elements of secondary structure. The inset in Figure 3 reports the difference spectrum obtained from the CD profiles of *Hb33−61a* in water at 70 and 10 °C. The presence of a positive and a negative band centered at about 194 and 218 nm, respectively, is compatible with the existence of some type of β-turn (*43*). A similar result has been observed also with indolicidin, another antibacterial linear peptide (*40*).

The near-UV spectra in aqueous solution and in the presence of SDS micelles (Figure 4) reveal that the peptide is able to undergo conformational transitions that involve also the spatial reorientation of the aromatic side chains. In water at 20 °C, we observe the two L_b bands typical of a Tyr residue exposed to the solvent at 282 nm and at ∼276 nm (*44*, *45*) while in the region 250−270 nm, we find two bands, 261 and 268 nm, that can be attributed to the Phe and His residues, respectively. In particular, the band at 261 nm can be attributed to the Phe L_b transition; its red shift, possibly, being the result of side-chain packing (*44*). Interestingly, at 37 °C, we detect only a broad negative band spanning from 259 to 288 nm that reflects an increased mobility with a consequent reduced spatial organization of the aromatic side chains.

The near-UV CD spectra in SDS clearly reveal that the aromatic side chains undergo a conformational rearrangement with respect to their conformation in water. The positive broad band spanning the region 270−290 nm can be attributed to the single Tyr residue. The presence of a shoulder at 289 nm and of a broad peak at 284 nm, each associated with a peak blue shifted by about 6−8 nm, suggests the presence of two populations of that tyrosine, one buried in the micelle and one exposed to the solvent (*44*, *46*). The band at 258 nm can be due to the L_b transition of the Phe residues while the one at 264 nm could be tentatively assigned to the His residues (*44*). At 37 °C, where the NMR measurements have been carried out, the overall spectral pattern is maintained. Nonetheless, it is worthwhile to note that while the band at 264 nm remains practically the same, the band at 258 nm and the broad band centered at about 278 nm are less intense. In addition, the fine structure of the Tyr band is almost lost.

Overall, the CD spectra show that *Hb33−61a* has a tendency to acquire elements of secondary structure in water at high temperature. Moreover, they indicate that the peptide interacts preferentially with negatively charged micelles, perhaps a better mimetic of the negatively charged outer surface of a bacterial cell wall, where it undergoes conformational changes that involve both the backbone and side-chain orientation.

NMR Measurements. On the basis of the CD results, the peptide structure was determined in the presence of SDS micelles at 37 °C. SDS has been selected, recognizing that, since a long time, it is widely accepted as a suitable model for amphiphilic systems when studying the structure of membrane binding peptides (*47*, *48*). In these experimental conditions the 2D ^{1}H NMR spectra of *Hb33−61a* exhibited acceptable sharp signals and a good chemical shift dispersion allowing unambiguous assignment of all of the proton resonances. It is worth noting that the peptide broad signals observed at 20 °C (data not shown) and sharpening at 37 °C, together with the absence of exchange cross-peaks in

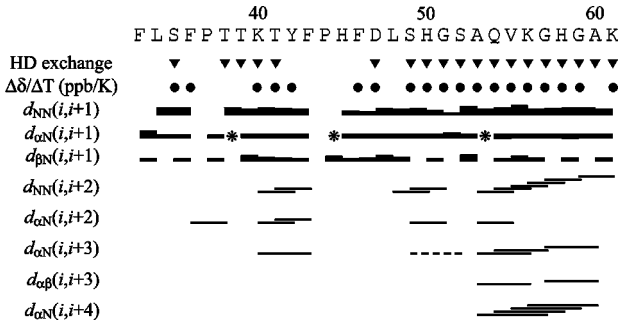

FIGURE 5: Summary of the sequential and medium-range NOE connectivities for 1.5 mM *Hb33−61a* in 200 mM SDS, pH 4.0, at 37 °C. The intensities of the observed NOEs are represented by the thickness of lines and were classified as strong, medium, and weak, corresponding to upper bound constraints of 2.5, 3.5, and 5 Å, respectively. The stars and the dashed line indicate potential NOE connectivities that could not be obtained due to resonance overlap. $\Delta\delta_{HN}/\Delta T$ = amide proton temperature coefficient. Filled circles indicate $|\Delta\delta_{HN}/\Delta T| < 6$ ppb/K. The symbol ▼ indicates the amide protons that do not exchange after 15 h from the addition of 90% D_2O/10% H_2O to the lyophilized peptide/SDS mixture.

any of the NMR experiments, provide a good indication that, in these experimental conditions, the peptide is bound to the micelles.

Sequential NMR Resonance Assignments. Sequential assignment was achieved by standard procedures (*49*). The ^1H chemical shifts and $^3J_{HN-\alpha}$ coupling constants have been submitted to BioMagRes Bank (accession number 6048).

The analysis of the pH dependence of the Hϵ1 resonance (*49*) of the His45, His50, and His58 imidazole ring, monitored by 2D ^1H NMR spectra, provided the unusually high pK_a of 7.7, 7.7, and 7.8, respectively. As for the two proline residues, the presence of NOEs between the Pro δH with the αH of the preceding residue indicates that the peptide bonds are in *trans* conformation.

Secondary Structure. The summary of the interresidue NOEs for the peptide is reported in Figure 5. It is recognized that when studying small peptides, NOEs allow to qualitatively highlight the coexistence of conformational families characterized by diverse secondary structure elements (*50*−*52*). As a result, while the concomitant presence of H^N-H^N and H^N-H^α connectivities indicates that the peptide is exploring β and α conformational regions, the presence of unfolded conformers impairs the possibility to use simply $d_{\alpha N}(i, i+1)$ connectivities to detect turns and loose helices. However, these structural elements can be detected by the presence of several medium-range interactions (*49*, *53*). In the case of *Hb33−61a*, the detection of $d_{\alpha N}(i, i+3)$ together with $d_{\alpha N}(i, i+2)$ connectivities is indicative of the presence of β-turns in the N-terminal and in the central region of the peptide. In particular, two type III β-turns spanning residues Lys40−Phe43 and Ser49−Ser52 were identified. On the other hand, the presence of medium-range $d_{\alpha N}(i, i+3)$ and $d_{\alpha N}(i, i+4)$ NOEs, together with the $d_{NN}(i, i+1)$ connectivities in the C-terminus, indicates the existence of a helical element spanning residues Ala53−Ala60. However, the coexistence throughout the peptide sequence of $d_{NN}(i, i+1)$ with $d_{\alpha N}(i, i+1)$ NOEs of comparable intensity, strongly suggests that the peptide backbone is affected by conformational fluctuations.

Molecular Modeling. A total of 173 nonredundant distance restraints, of which 62 were medium range, were used for structure calculation using DYANA. Out of the 100 structures generated, 40 were selected on the basis of their minimum target function (0.22 ± 0.02 Å^2) and energy minimized using the program DISCOVER. After minimization, 20 structures were selected on the basis of the low residual distance violation of their backbone. PROCHECK-NMR showed that all ϕ and ψ angles are in the allowed regions, and the global backbone RMSD (residues 33−61) turned out to be 1.63 ± 0.65 Å (Table 1). Figure 6 shows a cartoon depicting the stereoview of the NMR-derived minimum energy model. Interestingly, the selective superposition of the regions that present elements of secondary structure, residues Thr38−Phe43 and Ser49−Ala60 (Figure 7a,b), gives lower backbone RMSDs: 0.16 ± 0.11 and 0.25 ± 0.09 Å, respectively (Table 1). This result indicates that the peptide bound to SDS micelles consists of two, spatially independent, regions connected by a hinge encompassing residues Pro44−Phe48.

Table 1: Structure Statistics for the Ensemble of 20 *Hb33−61a* Structures in 200 mM SDS, pH 4.0, at 37 °C

	value
PROCHECK: Ramachandran plot analysis	
most favored region (%)	68.8
additionally allowed region (%)	28.5
generously allowed region (%)	2.7
disallowed region (%)	0
RMSD[a]	
backbone (all)	1.63 ± 0.65
backbone (residues 38−43)	0.16 ± 0.11
backbone (residues 44−48)	0.24 ± 0.07
backbone (residues 49−60)	0.25 ± 0.09
heavy atoms (all)	2.22 ± 0.77
heavy atoms (residues 38−43)	0.48 ± 0.16
heavy atoms (residues 44−48)	0.75 ± 0.26
heavy atoms (residues 49−60)	0.71 ± 0.23

[a] Root mean square deviation from pairwise comparison between all of the structures (Å).

H/D Exchange Experiments. Figure 8b,c reports the contour plots of the amide region of two TOCSY spectra obtained with the lyophilized sample of *Hb33−61a* bound to SDS micelles 5 h after it has been resuspended in 90% D_2O (the time required to obtain a TOCSY with good signal to noise in our experimental conditions) and after 20 h, respectively. Figure 8a is the spectrum of the SDS micelle-bound peptide in water, and it has been used as the "time 0" reference. The amide proton H/D exchange experiments reveal the existence of two major families of NHs: one corresponding to NHs that exchange in the first 5 h and another one corresponding to residues Ser35, Thr38−Thr41, Asp47, and Ser49−Lys61 that do not exchange even after 20 h (Figure 8c). The exception is residue Tyr42 that exchanges after about 10 h (Figure 8b). Figure 8d summarizes these results, evidencing that the exchangeable amide protons (yellow circles) are concentrated in the N-terminus, in particular in the joint region. The nonexchangeable amide protons are indicated in blue, and the Tyr42 NH, which exhibits an intermediate exchange rate, is indicated in red.

The coefficients ($\Delta\delta_{HN}/\Delta T$), representing the temperature dependence of the amide−proton chemical shifts of *Hb33−61a* when bound to SDS micelles, are in good agreement with the H/D exchange data and are reported in Figure 5. Values lower than 6 ppb/K are found in some N-terminal residues, Ser35−Phe36 and Lys40−Tyr42, and throughout the C-terminal half of the peptide. It is worth mentioning,

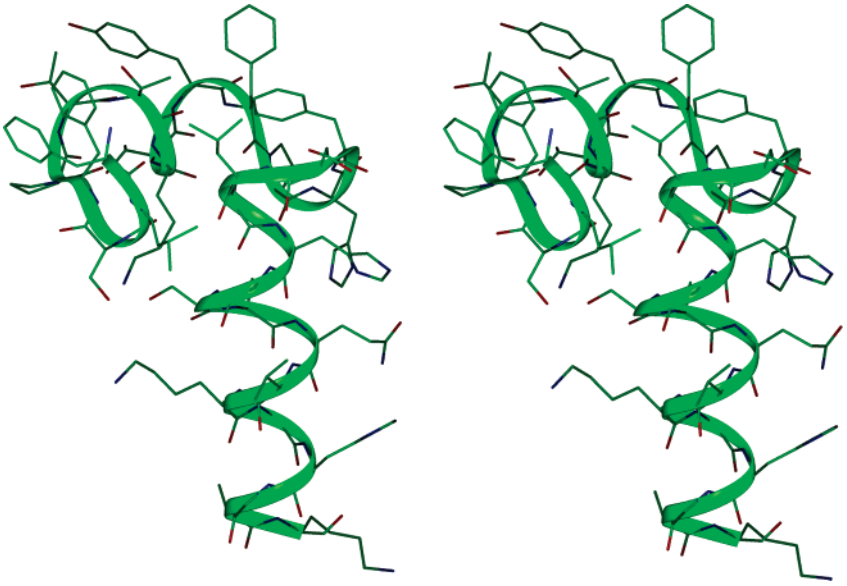

FIGURE 6: Stereoview of the minimum energy NMR-derived model of *Hb33−61a* bound to SDS micelles, pH 4.0, at 37 °C. The C-terminus is shown at the bottom.

however, that in these experimental conditions the reduced values of the $\Delta\delta_{HN}/\Delta T$ coefficients either might indicate that the NHs are protected from the solvent (*54*), being embedded in the micelle core, or might reflect the presence of secondary structure elements (*51*, *55*) or both.

DISCUSSION

The synthetic peptide *Hb33−61a*, that encompasses the region 33−61 of the bovine hemoglobin α-chain, was shown to have an antimicrobial activity selective against Gram-positive bacteria and fungi (*6*). While a more comprehensive description of the structural and functional differences between the amidated and carboxyl-free form of this peptide will be presented elsewhere, here we demonstrate that its biological activity can be related to its ability to permeabilize the bacterial membrane. Aiming to describe the molecular mechanism associated to this action and having verified the preferential affinity of the peptide for negatively charged surface, as a first step, we determined its structure when bound to SDS micelles. To avoid the possibility of peptide−peptide interaction, we used a 130-fold molar excess of SDS. Knowing that the SDS aggregation number is about 60, in these experimental conditions we end up with about two micelles per peptide molecule.

Hb33−61a Micelle-Bound Structure. The superposition of the N-terminal region, residues Thr38−Phe43 (Figure 7a), shows that two aromatic side chains are involved in hydrophobic interactions: Tyr42 and Phe43 with Thr38 and Thr39, respectively, as already suggested by the detection of interchain NOEs (Table 2). Inspection of the superposition of the C-terminal region, residues Ser49−Ala60 (Figure 7b), reveals the existence of an aromatic cluster involving the three His residues, all of them interacting with Gln54. The interaction of the His side chains with the Gln54 side chain carbonyl justifies their unusually high pK_a. Interestingly, His45 shows two preferential orientations. Also, in this case such a preferential spatial arrangement is confirmed by the presence of inter side chain NOEs (Table 2). Whether these chemical and structural features have a functional role we cannot say at the moment. Preliminary experiments using His45 methylated at Hε1 have failed to provide new clues (unpublished results). Finally, the superposition of the peptide portion that acts as a joint between the N- and C-terminal regions, residues Pro44−Asp48 (Figure 7c), evidences that also this part of the molecule possesses a preferred conformation. Though it does not present any conventional element of secondary structure, its structural organization is well defined due to the interaction of His45 with Pro44. This spatial arrangement, which corresponds also to the second preferential orientation of the His45 side chain, is supported by the detection of NOEs between Pro44 and His45 side chains (Table 2).

Table 2: NOEs Involving Aromatic Side Chains of *Hb33−61a* in 200 mM SDS, pH 4.0, at 37 °C

Thr38	Tyr42	His45	Gln54
Hγ	Hε	Hδ	Hε
Hγ	Hβ	His50	Gln54
Thr39	Phe43	Hε	Hε
Hβ	Hε	Hβ	Hβ
Hγ	Hε	Gln54	His58
Pro44	His45	Hε	Hδ
Hβ	Hδ	Hβ	Hβ
Hδ	Hβ		

Overall, the NMR-derived 3D structure of *Hb33−61a* (Figure 6) discloses the existence of a complex pattern of diverse intramolecular interactions that lead to an ordered spatial organization of the aromatic side chains distributed along the peptide sequence. The complexity of the structure, where a loose short helical stretch, two β-turns, and a number of aromatic residues with preferential orientations are present, justifies the shape of the observed CD spectra.

Hb33−61a and the Bovine Hemoglobin α-Chain. Figure 9a,b shows two superpositions of *Hb33−61a* on the corresponding sequence in the crystal structure of the bovine hemoglobin α-chain (PDB code 1G08). As can be seen, there is a good superposition for the helical stretch Ala53−Lys61, backbone RMSD 0.86 Å (Figure 9a), and for the region Tyr42−Phe46, backbone RMSD 1.09 Å (Figure 9b). It is remarkable to note that, especially for the region Tyr42−

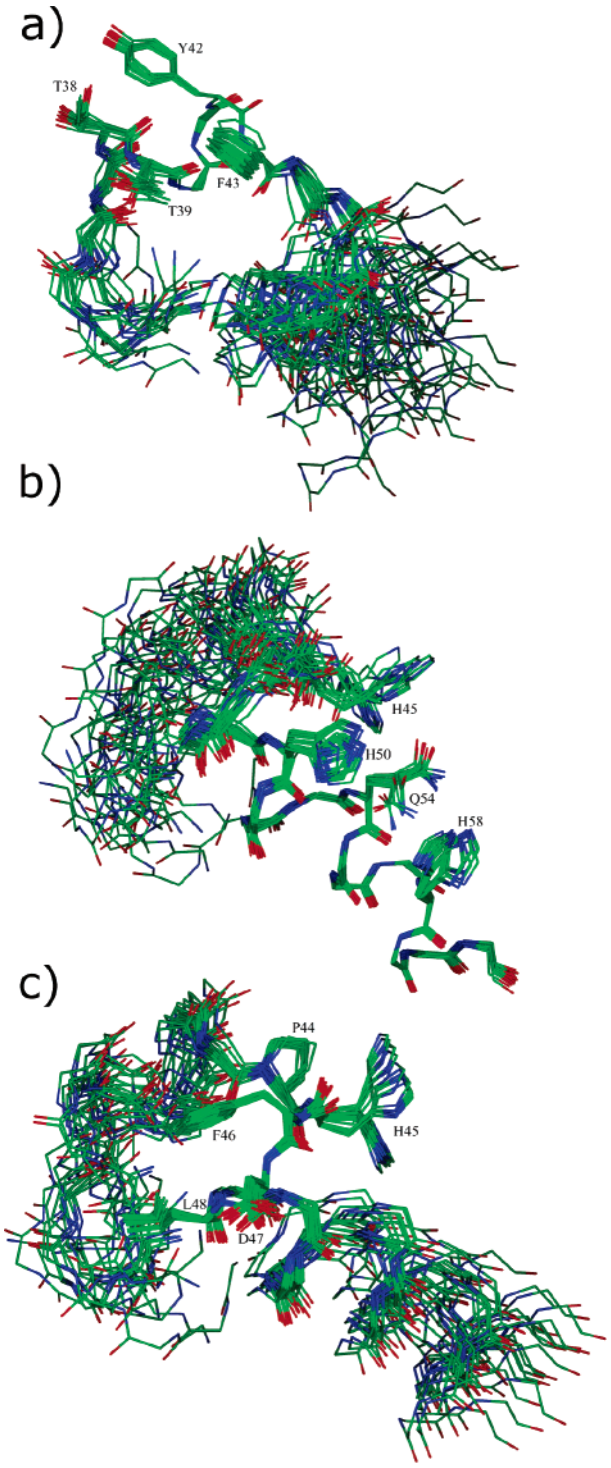

FIGURE 7: Superposition of the 20 minimum energy NMR-derived models of *Hb33−61a* bound to SDS micelles, pH 4.0, at 37 °C in (a) the N-terminus, residues Thr38−Phe43, (b) the C-terminus, residues Ser49−Ala60, and (c) the joint region, residues Pro44−Phe48. The C-terminus is always shown at the bottom.

Phe46, there is a very good match for the spatial orientation of the side chains of the aromatic residues. Overall, Figure 9c shows that *Hb33−61a* preserves the main elements of secondary and tertiary structure present in the hemoglobin α-chain (the helical stretch, residues Ala53−Lys61, and the aromatic cluster, residues Tyr42−Phe46, respectively) though with a different spatial organization. It is also interesting to note that a visual inspection of the aromatic residue location in the tetrameric hemoglobin reveals that, as in *Hb33−61a*, the only side chains that are exposed to the solvent are the ones of residues Pro44 and His45 (not shown).

Comparison with Other Peptides. The presence of a hinge or a joint connecting regions that possess elements of secondary structure seems to be a feature common to a number of antimicrobial peptides. NK-2, a short and potent antibiotic derived from the porcine NK-lysin, very effective against *Candida* as well as against several bacterial strains at micromolar concentration, has been suggested to possess a helix−hinge−helix conformation (*56*). Cecropin A, active against a variety of Gram-positive and Gram-negative bacteria, had its structure determined in hexafluoroisopropyl alcohol and showed a helix−loop−helix conformation: one helix being amphipathic while the other highly hydrophobic (*57*). A similar type of turn-like structure is exhibited also by tritrpticin, a member of the cathelicidin family characterized by a high content of Trp residues. In this case, however, there are no amphipathic helical regions, and the ability to bind to the bacterial membrane is associated to the presence of a cluster of aromatic residues (*58*). Indolicidin is an antimicrobial peptide, characterized by a noncanonical secondary structure though presenting a bent conformation and, in its central part, exhibiting an hydrophobic core rich in aromatic residues (*59*). All of these peptides are able, in some way, to insert into the hydrophobic core of a bilayer or a micelle. In the case of the cecropin peptides, it has been invoked the lack of a certain degree of flexibility in the region connecting the hydrophobic C-terminus and the more polar N-terminus to justify the preferential localization of cecropin P1 at the bilayer surface (*60*).

Interestingly, it has also been reported that peptides characterized by a similar molecular architecture may exhibit biological activity other than the antimicrobial one. A peptide from the herpex simplex virus protein ICP47 has been proved to be able to block antigen presentation (*53*). Recently, it has been shown that the chimeric 32-residue peptide, PNC-27, resulting from the combination of segment 12−26 of the protein p53, involved in cell cycle control and apoptosis signaling, with the penetratin peptide, from the *Drosophila* homeobox protein *Antennapedia* penetratin, exhibits an U-shaped structure reminiscent of an helix−loop−helix motif, and it is able to selectively kill cancer cells (*61*).

Location of Hb33−61a in the SDS Micelle. The absence of H/D exchange observed for those NHs that are also characterized by a reduced value of the chemical shift temperature coefficients (Figures 5 and 8), together with the spectral features observed in the near-UV CD spectra (Figure 4), suggests that only certain regions of *Hb33−61a* penetrate the micellar surface. In this respect, the longer time required by the Tyr42 NH NMR resonance to disappear in the H/D exchange experiment is consistent with the hypothesis, suggested by the near-UV CD spectra, that the residue may exist in two preferential orientations: one more exposed and one less exposed to the solvent. Its possible functional significance is being investigated. On the basis of this experimental evidence in Figure 10 is presented a cartoon that depicts the possible location of *Hb33−61a* relative to a schematic SDS micelle represented as a sphere. The size of the peptide has been obtained from the NMR-derived structure while, for a spherical SDS micelles, we considered a diameter of about 35 Å (*62*). The color coding of the amide

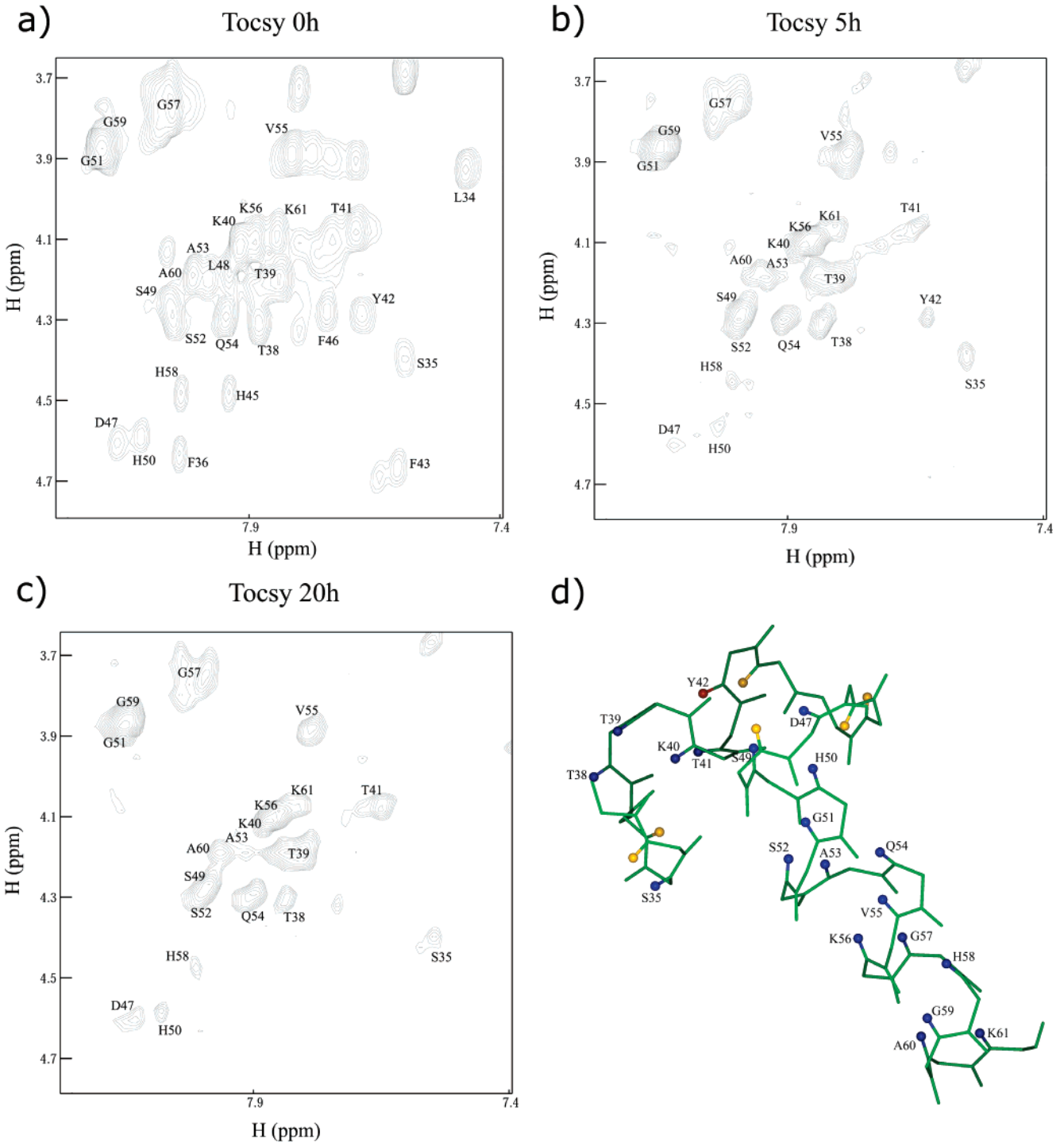

FIGURE 8: Contour plots of the amide region of TOCSY spectra obtained from (a) 1.5 mM *Hb33−61a* in 200 mM SDS, pH 4.0, at 37 °C (this spectrum has been used as the time 0 reference). Panels b and c represent the amide region of TOCSY spectra of lyophilized 1.5 mM *Hb33−61a* in 200 mM SDS, pH 4.0, at 37 °C; after 5 h it was dissolved in 90% D_2O/10% H_2O and after 20 h, respectively. Panel d is a cartoon showing exchanging (yellow circles) and not exchanging (blue circles) amide protons. The Tyr42 amide proton is indicated in red because it exchanges after about 10 h. The C-terminus is always shown at the bottom.

protons is the same used in the NMR H/D exchange experiments (Figure 8d).

Another chimeric 27-residue peptide formed by the fusion of residues 1−12 of the neuropeptide galanin with mastoparan, and called transportan, has been reported to exhibit high affinity for SDS micelles, and its proposed structure and location in such a membrane mimetic medium are quite similar to the one we have found for *Hb33−61a*. In fact, it possesses an N-terminal region, located just below the micelle−water interface, that is characterized by the presence of turn elements followed by a bend exposed to the solvent and by an α-helical structure in the C-terminus deeply embedded into the micelle (*48*). A similar structure has recently been found also when it interacts with bicelles (*63*). It is remarkable to note that transportan is able to cross the cell membrane of several cell lines transporting cargo molecules and to enter the cell nucleus where it eventually exerts its activity (*64*).

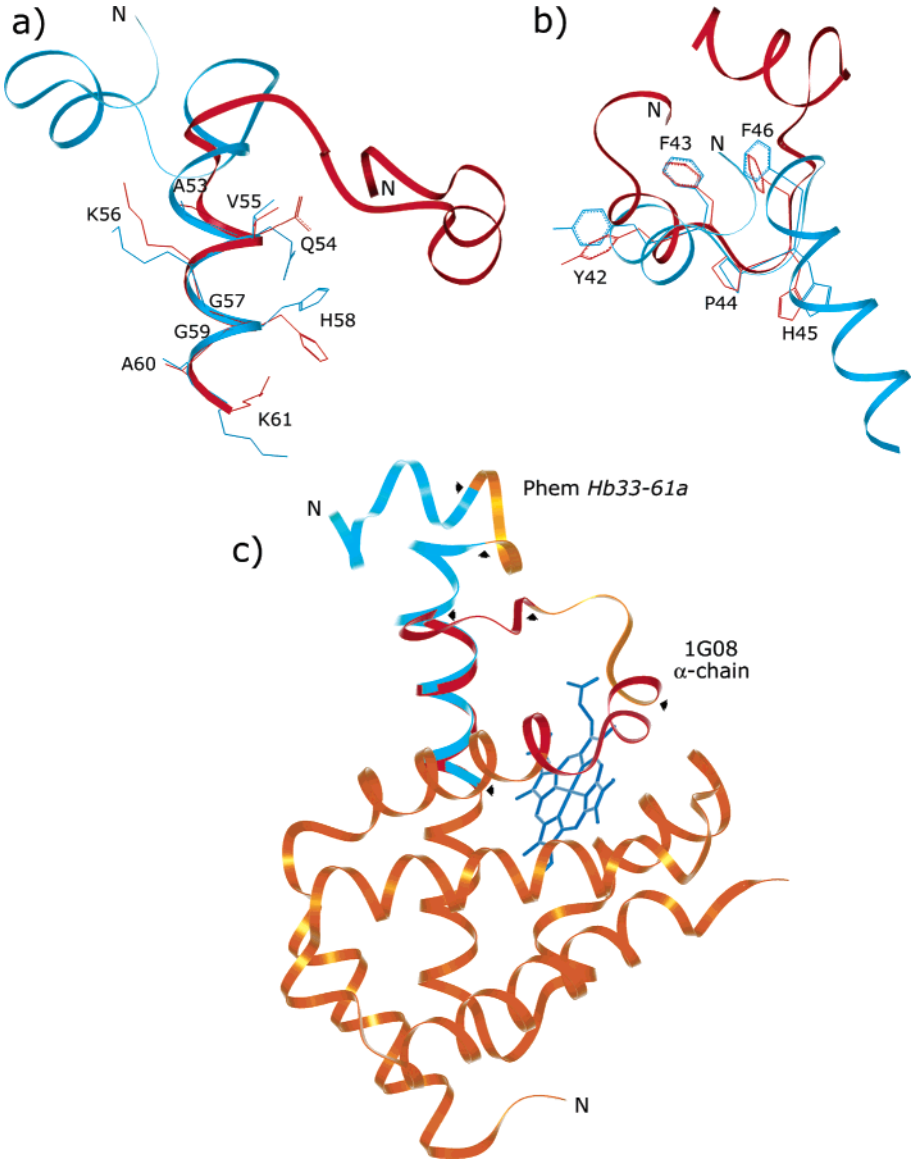

FIGURE 9: Comparison between segments of the minimum energy NMR-derived model of *Hb33−61a* bound to SDS micelles, pH 4.0, at 37 °C (blue) with the corresponding regions in the crystal structure of the bovine hemoglobin α-chain (PDB code 1G08; red/orange). Superposition of (a) residues Ala53−Lys61 and (b) residues Tyr42−Phe46 and (c) overall representation of *Hb33−61a* and bovine hemoglobin α-chain superposed on residues Ala53−Lys61. Arrows identify the regions of superposition in panels a and b: *Hb33−61a* (blue/yellow); hemoglobin α-chain (yellow/red).

Hb33−61a Surface Features. Inspection of the molecular surface of *Hb33−61a* using the program Insight II (Figure 11a) evidences the existence of hydrophobic patches all along one side of the peptide and of a polar strip extending over the peptide length on the other side. Despite this, the peptide cannot really be defined as amphipathic because there is no clear separation between hydrophobic and polar residues. In addition, when the MOLMOL program (*65*) is used to represent the average surface charge distribution (Figure 11b), it turns out that the peptide is mostly positively charged, thus justifying its specific affinity for negatively charged surface.

CONCLUSIONS

The positive character of the peptide and the specific affinity for negatively charged micelles indicate that the driving force of the interaction is primarily electrostatic, thus suggesting that, as observed for peptides with potency at micromolar concentration, indeed the target of *Hb33−61a* is the lipid membrane and not a specific receptor (*66*).

The possibility to superimpose independently various regions of the ensemble of the NMR-derived solution structures, leaving the remaining portion of the peptide somewhat spatially dispersed (Figure 7a,b), suggests that when bound to a membrane-like environment, the N- and C-terminal regions of *Hb33−61a* are able to move independently, with the segment Pro44−Leu48 acting as an hinge. Such a structural flexibility might be partly responsible for the ability of the peptide to permeate the bacterial membrane as hypothesized for other AMPs (*60*).

Finally, the fact that *Hb33−61a* preserves the main structural features present in the corresponding sequence of the bovine hemoglobin α-chain though with a different spatial organization supports the hypothesis that hemoglobin encodes in its primary and secondary structure a number of

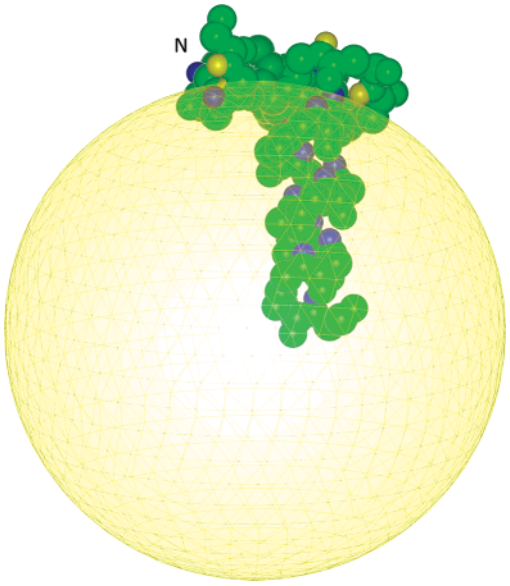

FIGURE 10: Cartoon depicting the localization of *Hb33−61a* in a schematic SDS micelle represented as a sphere. The peptide dimensions have been taken from the NMR-derived structure of this work. Only the N-terminus is indicated. The diameter of the spherical SDS micelle has been considered to be 35 Å (*62*). Yellow balls represent the solvent fast exchanging amide protons, while blue balls indicate the nonexchanging ones as derived from the NMR H/D exchange experiments.

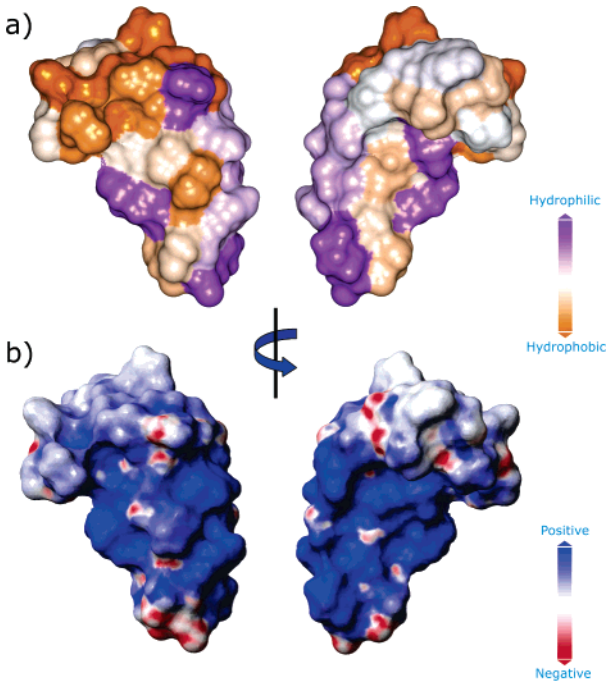

FIGURE 11: (a) Hydrophobic/polar surface obtained using Insight II and (b) potential surface describing the average positive and negative surface charge obtained using MOLMOL (*65*). The C-terminus is at the bottom. The two images on the right side of panels a and b are obtained by 180° rotation around the axis indicated in the center of the figure.

additional biological functions that are released through proteolysis (*25*).

In conclusion, we believe that *Hb33−61a* constitutes an interesting model to progress in the understanding of the molecular basis of AMP's biological activity. Structural and functional studies are in progress on truncated analogues in order to identify the core of the peptide antimicrobial activity.

ACKNOWLEDGMENT

We thank Dr. R. Schneider for donation of the Live/Dead BacLight viability stain.

SUPPORTING INFORMATION AVAILABLE

One figure showing the least-squares fit to the Henderson−Hasselbach equation of the pH dependence of the Hϵ1 resonance (*49*) of the His45, His50, and His58 imidazole ring, monitored by TOCSY ^{1}H NMR spectra. This material is available free of charge via the Internet at http://pubs.acs.org.

REFERENCES

1. Hancock, R. E. W., and Lehrer, R. (1998) Cationic peptides: a new source of antibiotics, *Trends Biotechnol. 16*, 82−88.
2. Hancock, R. E. W. (1997) Peptide antibiotics, *Lancet 349*, 418−422.
3. van't Hof, W., Veerman, E. C. I., Helmerhorst, E. J., and Amerongen, A. V. N. (2001) Antimicrobial peptides: properties and applicability, *Biol. Chem. 382*, 597−619.
4. Hancock, R. E. W., and Scott, M. G. (2000) The role of antimicrobial peptides in animal defenses, *Proc. Natl. Acad. Sci. U.S.A. 97*, 8856−8861.
5. Farnaud, S., and Evans, R. W. (2003) Lactoferrin—a multifunctional protein with antimicrobial properties, *Mol. Immunol. 40*, 395−405.
6. Fogaça, A. C., Silva, P. I., Jr., Miranda, M. T. M., Bianchi, A. G., Miranda, A., Ribolla, P. E. M., and Daffre, S. (1999) Antimicrobial activity of a bovine hemoglobin fragment in the tick *Boophilus microplus*, *J. Biol. Chem. 274*, 25330−25334.
7. Nakajima, Y., Ogihara, K., Taylor, D., and Yamakawa, M. (2003) Antibacterial hemoglobin fragments from the midgut of the soft tick, *Ornithodoros moubata* (Acari: Argasidae), *J. Med. Entomol. 40*, 78−81.
8. Liepke, C., Baxmann, S., Heine, C., Breithaupt, N., Standker, L., and Forssmann, W. G. (2003) Human hemoglobin-derived peptides exhibit antimicrobial activity: a class of host defense peptides, *J. Chromatogr., Sect. B: Anal. Technol. Biomed. Life Sci. 791*, 345−356.
9. Hancock, R. E. W., and Diamond, G. (2000) The role of cationic antimicrobial peptides in innate host defences, *Trends Microbiol. 8*, 402−410.
10. Koczulla, A. R., and Bals, R. (2003) Antimicrobial peptides: current status and therapeutic potential, *Drugs 63*, 389−406.
11. Epand, R. M., and Vogel, H. J. (1999) Diversity of antimicrobial peptides and their mechanisms of action, *Biochim. Biophys. Acta 1462*, 11−28.
12. Dathe, M., and Wieprecht, T. (1999) Structural features of helical antimicrobial peptides: their potential to modulate activity on model membranes and biological cells, *Biochim. Biophys. Acta 1462*, 7−87.
13. Zhang, L., Rozek, A., and Hancock, R. E. W. (2001) Interaction of cationic antimicrobial peptides with model membranes, *J. Biol. Chem. 276*, 35714−35722.
14. Vaara, M. (1992) Agents that increase the permeability of the outer membrane, *Microbiol. Rev. 56*, 395−411.
15. Hancock, R. E. W., Falla, T., and Brown, M. (1995) Cationic bactericidal peptides, *Adv. Microb. Physiol. 37*, 135−175.
16. Yeaman, M. R., and Yount, N. Y. (2003) Mechanisms of antimicrobial peptide action and resistance, *Pharmacol. Rev. 55*, 27−55.
17. Pellegrini, A., Dettling, C., Thomas, U., and Hunziker, P. (2001) Isolation and characterization of four bactericidal domains in the bovine beta-lactoglobulin, *Biochim. Biophys. Acta 1526*, 131−140.
18. Oevermann, A., Engels, M., Thomas, U., and Pellegrini, A. (2003) The antiviral activity of naturally occurring proteins and their peptide fragments after chemical modification, *Antiviral Res. 59*, 23−33.
19. Zucht, H. D., Raida, M., Adermann, K., Mägert, H. J., and Forssmann, W. G. (1995) Casocidin-I: a casein-alpha s2 derived peptide exhibits antibacterial activity, *FEBS Lett. 372*, 185−188.

20. Bellamy, W., Takase, M., Yamauchi, K., Wakabayashi, H., Kawase, K., and Tomita, M. (1992) Identification of the bactericidal domain of lactoferrin, *Biochim. Biophys. Acta 1121*, 130−136.
21. van der Kraan, M. I. A., Groenink, J., Nazmi, K., Veerman, E. C. I., Bolscher, J. G. M., and Amerongen, A. V. N. (2004) Lactoferrampin: a novel antimicrobial peptide in the N1-domain of bovine lactoferrin, *Peptides 25*, 177−183.
22. Pellegrini, A., Hulsmeier, A. J., Hunziker, P., and Thomas, U. (2004) Proteolytic fragments of ovalbumin display antimicrobial activity, *Biochim. Biophys. Acta 1672*, 76−85.
23. Parish, C. A., Jiang, H., Tokiwa, Y., Berova, N., Nakanishi, K., McCabe, D., Zuckerman, W., Xia, M. M., and Gabay, J. E. (2001) Broad-spectrum antimicrobial activity of hemoglobin, *Bioorg. Med. Chem. 9*, 377−382.
24. Froidevaux, R., Krier, F., Nedjar-Arroume, N., Vercaigne-Marko, D., Kosciarz, E., Ruckebusch, C., Dhulster, P., and Guillochon, D. (2001) Antibacterial activity of a pepsin-derived bovine hemoglobin fragment, *FEBS Lett. 491*, 159−163.
25. Ivanov, V. T., Karelin, A. A., Nazimov, I. V., and Pletnev, V. Z. (1997) Hemoglobin as a source of endogenous bioactive peptides: the concept of tissue-specific peptide pool, *Biopolymers 43*, 171−188.
26. Fogaça, A. C. (2003) Purificação e caracterização de peptídeos antimicrobianos do carrapato de boi *Boophilus microplus*, Ph.D. Thesis.
27. Silva, P. I., Jr., Daffre, S., and Bulet, P. (2000) Isolation and characterization of gomesin, an 18-residue cysteine-rich defense peptide from the spider *Acanthoscurria gomesiana* hemocytes with sequence similarities to horseshoe crab antimicrobial peptides of the tachyplesin family, *J. Biol. Chem. 275*, 33464−33470.
28. Andreu, D., and Rivas, L. (1998) Animal antimicrobial peptides: an overview, *Biopolymers 47*, 415−433.
29. Sforça, M. L., Oyama, S., Jr., Canduri, F., Lorenzi, C. C. B., Pertinhez, T. A., Konno, K., Souza, M. B., Palma, M. S., Neto, J. R., Azevedo, W. F., Jr., and Spisni, A. (2004) How C-terminal carboxyamidation alters the biological activity of peptides from the venom of the eumenine solitary wasp, *Biochemistry 43*, 5608−5617.
30. Braunschweiler, L., and Ernst, R. R. (1983) Coherence transfer by isotropic mixing: application to proton correlation spectroscopy, *J. Magn. Reson. 53*, 521−528.
31. Jeener, J., Meier, B. H., Bachmann, P., and Ernst, R. R. (1979) Investigation of exchange processes by two-dimensional NMR spectroscopy, *J. Chem. Phys. 71*, 4546−4553.
32. Rance, M., Sørensen, O., Bodenhausen, G., Wagner, G., Ernst, R. R., and Wüthrich, K. (1983) Improved spectral resolution in cosy ^{1}H NMR spectra of proteins via double quantum filtering, *Biochem. Biophys. Res. Commun. 117*, 479−485.
33. Pristovšek. P., Rüterjans, H., and Jerala, R. (2002) Semiautomatic sequence-specific assignment of proteins based on the tertiary structure: The program st2 NMR, *J. Comput. Chem. 23*, 335−340.
34. Chang, D.-K., Cheng, S.-F., Trivedi, V. D., and Yang, S.-H. (2000) The amino-terminal region of the fusion peptide of influenza virus hemagglutinin HA2 inserts into sodium dodecyl sulfate micelle with residues 16−18 at the aqueous boundary at acidic pH. Oligmerization and the conformational flexibility, *J. Biol. Chem. 275*, 19150−19158.
35. Güntert, P., Mumenthaler, C., and Wüthrich, K. (1997) Torsion angle dynamics for NMR structure calculation with the new program Dyana, *J. Mol. Biol. 273*, 283−298.
36. Dauber-Osguthorpe, P., Roberts, V. A., Osguthorpe, D. J., Wolff, J., Genest, M., and Hagler, A. T. (1988) Structure and energetics of ligand binding to proteins: *E. coli* dihydrofolate reductase-trimethoprim, a drug-receptor system, *Proteins: Struct., Funct., Genet. 4*, 31−47.
37. Laskowsky, R. A., Rullmann, J. A., MacArthur, M. W., Kaptein, R., and Thorton, J. M. (1996) AQUA and PROCHECK-NMR: programs for checking the quality of protein structures solved by NMR, *J. Biomol. NMR 8*, 477−486.
38. Yang, J. J., Pitkeathly, M., and Radford, S. E. (1994) Far-UV circular dichroism reveals a conformational switch in a peptide fragment from the beta-sheet of hen lysosyme, *Biochemistry 33*, 7345−7353.
39. Woody, R. W. (1994) Contributions of tryptophan side chains to the far-ultraviolet circular dichroism of proteins, *Eur. Biophys. J. 23*, 253−262.
40. Ladokhin, A. S., Selsted, M. E., and White, S. H. (1999) CD spectra of indolicidin antimicrobial peptides suggest turns, not polyproline helix, *Biochemistry 38*, 12313−12319.
41. Chen, Y. H., Yang, J. T., and Chau, K. H. (1974) Determination of the helix and beta-form of proteins in aqueous solution by circular dichroism, *Biochemistry 13*, 3350−3359.
42. Pertinhez, T. A., Krybus, R., Cilli, M. E., Paiva, A. C. M., Nakaie, C. R., Franzoni, L., Sartor, G., Spisni, A., and Schreier, S. (2002) Conformational flexibility of three cytoplasmic segments of the angiotensin II AT_{1A} receptor: a circular dichroism and fluorescence spectroscopy study, *J. Pept. Sci. 8*, 23−35.
43. Woody, R. W. (1974) in *Peptides, Polypeptides and Proteins* (Blout, E. R., Bovey, F. A., Goodman, M., and Lotan, N., Eds.) pp 338−350, John Wiley & Sons, New York.
44. Woody, R. W. (1996) in *Circular Dichroism and the Conformational Analysis of Biomolecules* (Fasman, G. D., Ed.) pp 110−144, Plenum Press, New York.
45. Sreerama, S., Manning, M. C., Powers, M. E., Zhang, J.-X., Goldenberg, D. P., and Woody, R. W. (1999) Tyrosine, phenylalanine, and disulfide contributions to the circular dichroism of proteins: circular dichroism spectra of wild-type and mutant bovine pancreatic trypsin inhibition, *Biochemistry 38*, 10814−10822.
46. Donovan, J. W. (1969) Ultraviolet absorption by proteins, in *Physical Principle and Techniques in Protein Chemistry* (Leach, S. J., Ed.) Part A, pp 101−170, Academic Press, New York.
47. Henry, G. D., and Sykes, B. D. (1994) Methods to study membrane protein structure in solution, *Methods Enzymol. 239*, 515−535.
48. Lindberg, M., Jarvez, J., Langel, Ü., and Gräslund, A. (2001) Secondary structure and position of the cell-penetrating peptide transportan in SDS micelles as determined by NMR, *Biochemistry 40*, 3141−3149.
49. Wüthrich, K. (1986) *NMR of Proteins and Nucleic Acids*, John Wiley & Sons, Zürich.
50. Dyson, H. J., Rance, M., Houghten, R. A., Wright, P. E., and Lerner, R. A (1988) Folding of immunogenic peptide fragments of proteins in water solution. II. The nascent helix, *J. Mol. Biol. 201*, 201−217.
51. Dyson, H. J., Rance, M., Houghten, R. A., Lerner, R. A., and Wright, P. E. (1988) Folding of immunogenic peptide fragments of proteins in water solution. I. Sequence requirements for the formation of a reverse turn, *J. Mol. Biol. 201*, 161−200.
52. de Chiara, C., Nicastro, G., Spisni, A., Zanotti, F., Cocco, T., and Papa, S. (2002) Activity and NMR structure of synthetic peptides of the bovine ATPase inhibitor protein, IF1, *Peptides 23*, 2127−2141.
53. Pfänder, R., Neumann, L., Zweckstetter, M., Seger, C., Holak, A. T., and Tampé, R. (1999) Structure of the active domain of the herpes simplex virus protein ICP47 in water/sodium dodecyl sulfate solution determined by nuclear magnetic resonance spectroscopy, *Biochemistry 38*, 13692−13698.
54. Rothemund, S., Weisshoff, H., Beyermann, M., Krause, E., Bienert, M., Mügge, C., Sykes, B. D., and Sönnichsen, D. (1996) Temperature coefficients of amide proton NMR resonance frequencies in trifluoroethanol: a monitor of intramolecular hydrogen bonds in helical peptides, *J. Biomol. NMR 8*, 93−97.
55. Baxter, N. J., and Williamson, M. P. (1997) Temperature dependence of ^{1}H chemical shifts in proteins, *J. Biomol. NMR 9*, 359−369.
56. Schröder-Borm, H., Willumeit, R., Brandenburg, K., and Andrä, J. (2003) Molecular basis for membrane selectivity of NK-2, a potent peptide antibiotic derived from NK-lysin, *Biochim. Biophys. Acta 1612*, 164−171.
57. Holak, T. A., Engström, A., Kraulis, P. J., Lindeberg, G., Bennich, H., Jones, A., Gronenborn, A. M., and Clore, M. G. (1988) The solution conformation of the antibacterial peptide cecropin A: a nuclear magnetic resonance and dynamical simulated annealing study, *Biochemistry 27*, 7620−7629.
58. Schibli, D. J., Hwang, P. M., and Vogel, H. J. (1999) Structure of the antimicrobial peptide tritrpticin bound to micelles: a distinct membrane-bound peptide fold, *Biochemistry 38*, 16749−16755.
59. Rozek, A., Friedrich, C. L., and Hancock, R. E. W. (2000) Structure of the bovine antimicrobial peptide indolicidin bound to dodecylphosphocholine and sodium dodecyl sulfate micelles, *Biochemistry 39*, 15765−15774.
60. Gazit, E., Miller, I. R., Biggin, P. C., Samson, M. S. P., and Shai, Y. (1996) Structure and orientation of the mammalian antibacterial peptide cecropin P1 within phospholipid membranes, *J. Mol. Biol. 258*, 860−870.

61. Rosal, R., Pincus, M. W., Brandt-Rauf, P. W., Fine, R. L., Michl, J., and Wang, H. (2004) NMR solution structure of a peptide from the mdm-2 binding domain of the p53 protein that is selectively cytotoxic to cancer cells, *Biochemistry 43*, 1845−1861.
62. Törnblom, M., Henriksson, U., and Ginley, M. (1994) A field dependent H-2 nuclear magnetic relaxation study of the aggregation behavior in micellar solutions of CTAB and SDS, *J. Phys. Chem. 98*, 7041−7051.
63. Bárány-Wallje, E., Andersson, A., Gräslund, A., and Mäler, L. (2004) NMR solution structure and position of transportan in neutral phospholipid bicelles, *FEBS Lett. 567*, 265−269.
64. Derossi, D., Chassaing, G., and Prochiantz, A. (1998) Trojan peptides: the penetratin system for intracellular delivery, *Trends Cell Biol. 8*, 84−87.
65. Koradi, R., Billeter, M., and Wüthrich, K. (1996) MOLMOL: a program for display and analysis of macromolecular structures, *J. Mol. Graphics 14*, 51−55.
66. Shai, Y. (2002) From innate immunity to de-novo designed antimicrobial peptides, *Curr. Pharm. Des. 8*, 715−725.

BI0475323